Ab initio molecular dynamics study of the reactions of allene cation induced by intense 7 micron laser pulses

Yi-Jung Tu & H. Bernhard Schlegel

Taylor & Francis
Taylor & Francis Group

Check for updates

DIETER CREMER MEMORIAL

Ab initio molecular dynamics study of the reactions of allene cation induced by intense 7 micron laser pulses

Yi-Jung Tu and H. Bernhard Schlegel

Department of Chemistry, Wayne State University, Detroit, MI, USA

ABSTRACT

The isomerisation and fragmentation of allene cation ($H_2C = C = CH_2^+$) by short, intense laser pulses were simulated by Born-Oppenheimer molecular dynamics (BOMD) on the ground state potential energy surface using the B3LYP/6-31 + G(d,p) level of theory and a 10 cycle 7 μm cosine squared pulse with a maximum field strength of 0.07 au. Laser fields polarised along the $C = C = C$ axis deposits an average of 150 kcal/mol in the molecule, compared to only 25 and 51 kcal/mol for perpendicular polarisations. Approximately 90% of the trajectories with the field aligned with the $C = C = C$ axis underwent one or more structural rearrangement steps to form $H_2C = CH–CH^+$ (15%), H_3CCCH^+ (4%), cyclopropene cation (6%), and allene cation with rearranged hydrogens and carbons (47%). In addition, a variety of fragments including $H_2CCCH^+ + H$ (10%), $c-C_3H_3^+ + H$ (7%), and $HCCCH^+ + H_2$ (2%) trajectories were produced after isomerisation. With the same amount of thermal energy, field-free BOMD shows good agreements with the BOMD with the field. However, RRKM calculations favour isomerisation to propyne cation and dissociation to $HCCCH^+ + H_2$. This suggests that for molecules in intense laser fields the energy in the intermediate isomers is not distributed statistically.
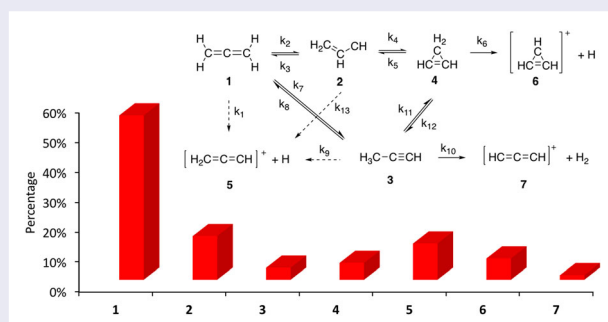
Introduction

Yamanouchi and co-workers have studied hydrogen migration and fragmentation of allene and propyne cations driven by ultra-short, intense laser pulses [1–8]. In experiments using 800 nm pump-probe coincidence momentum imaging, they found ultra-fast hydrogen migration, fragmentation and H_n^+ ejection. Mebel and Bandrauk have thoroughly investigated the potential energy surface (PES) of allene cations [9], showing that allene cation ($CH_2 = C = CH_2^+$) can isomerise to vinylmethylene cation ($CH_2 = CH–CH^+$), propyne cation (CH_3CCH^+), and cyclopropene cation ($c-C_3H_4^+$), and

these isomers can dissociate to $H_2CCCH^+ + H$, $c-C_3H_3^+ + H$, and $HCCCH^+ + H_2$. In earlier work, we found that 7 μm laser pulses couple more strongly with molecular vibrations than 800 nm pulses, and can lead to extensive isomerisation and fragmentation [10–14]. These investigations also showed that intense 7 μm laser pulses are able to selectively enhance specific reaction channels for aligned molecules by depositing energy in a non-statistical manner [10–14]. In a previous study [15], we examined the fragmentation of allene dication on the singlet and triplet surfaces using the Born-Oppenheimer ab initio classical trajectory calculations. In this work,

we present a Born-Oppenheimer molecular dynamics (BOMD) study of the isomerisation and fragmentation reactions of allene cation in a mid-IR laser field. Our goal is to explore the branching ratios of aligned allene cation when it interacts with the short, intense laser pulses. The branching ratios were also calculated using RRKM (Rice-Ramsperger-Kassel-Marcus) theory in order to compare the strong field dynamics with yields of isomerisation and fragmentation reaction of allene cation assuming statistical distributions of vibrational energy.

Computational methods

All calculations were performed with the development version of the Gaussian program [16]. The geometries of allene cation (**1**), its isomers (**2**, **3**, and **4**), transition states, and dissociation products (**5**, **6**, and **7**) were optimised at the B3LYP/6-31 + G(d,p) level of theory. The transition state structures have one imaginary frequency, and the reactant, intermediate isomers, and dissociation products have no imaginary frequencies. Classical trajectories were carried out on the ground state Born-Oppenheimer surface in the oscillating electric field of a laser pulse. After testing various laser parameters of field strength, pulse length, and field polarisations, we chose a 7 μm laser pulse with a maximum field strength of 0.07 au and aligned with the $C = C = C$ axis of allene cation to simulate the isomerisation and fragmentation processes. The trajectories were started from the optimised geometry of allene cation and calculated at the B3LYP/6-31 + G(d,p) level of theory using the Hessian-based predictor-corrector algorithm [17] with a step size of 0.25 fs and Hessian updating [18,19] for 20 steps before recalculation. The trajectory initial conditions were constructed using the microcanonical normal mode

sampling of the zero-point energy [20]. For comparison, the field-free BOMD trajectories were also computed by adding the same amount of energy as that gained on average from the laser pulse and using the normal mode sampling.

To estimate branching ratios assuming a statistical distribution of the vibrational energy in the various isomers and fragments, the rates for the reactions were also calculated using the RRKM theory. For a unimolecular reaction, the RRKM rate constant with an internal energy, $k(E)$, can be expressed as:

$$k(E) = \frac{\sigma N^{\#}(E - E^{\#})}{N(E)}$$

where E is the internal energy of the system, $E^{\#}$ is the activation energy for the reaction, $N^{\#}(E - E^{\#})$ is the total number of states of the transition state with energy less than or equal to $E - E^{\#}$, and the density of states, $N(E)$, is the number of states of the reactant or intermediate per energy interval. $N^{\#}(E - E^{\#})$ and $N(E)$ were calculated using the direct count method of Beyer and Swinehart [21]. There are 15 vibrational frequencies for allene cation and its isomers and 14 vibrational frequencies for the corresponding transition states. The vibrational data used for RRKM calculation is listed in Table 1. Scheme 1 shows all possible reaction steps considered in RRKM calculations. The rate constants for all reaction steps were weighted by reaction symmetry (σ). For example, allene cation has four hydrogen atoms that can undergo 1,2 hydrogen migration, so the k_2 rate constant was multiplied by four. The RRKM rate constants were used in the integration of the reaction kinetics (Scheme 1) to obtain the relative abundance of various isomers and dissociation products as a function of time.

Table 1. Relative energies[a] and vibrational frequencies of intermediates and the transition state at the B3LYP/6-31 + G(d,p) level of theory.

Structure[a]	Relative E[b] (kcal/mol)	Frequency (cm^{-1})
1	0	326, 346, 796, 800, 915, 935, 1005, 1070, 1359, 1406, 1652, 3079, 3096, 3175, 3178
2	25.5	299, 388, 662, 808, 992, 1025, 1140, 1281, 1286, 1494, 1577, 3146, 3174, 3225, 3257
3	16.0	125, 345, 437, 614, 698, 896, 983, 1212, 1285, 1428, 2084, 2877, 2996, 3088, 3365
4	24.1	393, 568, 702, 824, 900, 921, 1019, 1027, 1132, 1313, 1562, 2934, 2966, 3238, 3279
TS(1/2)	31.3	295, 386, 568, 722, 834, 894, 1060, 1153, 1479, 1644, 2809, 3178, 3286, 3303
TS(1/3)	40.6	207, 377, 494, 563, 674, 923, 1024, 1054, 1439, 1931, 2518, 3127, 3251, 3372
TS(2/4)	27.7	370, 645, 777, 796, 927, 958, 1124, 1218, 1453, 1610, 3116, 3188, 3238, 3336
TS(3/4)	74.9	207, 377, 494, 563, 674, 923, 1024, 1054, 1439, 1931, 2518, 3127, 3251, 3372
TS(3/7)	69.9	211, 272, 343, 408, 413, 488, 521, 849, 979, 1288, 1953, 3344, 3367, 4097
TS(4/6)	49.1	265, 459, 790, 912, 940, 985, 1006, 1032, 1277, 1305, 1643, 3252, 3262, 3304
TS(1/5)[c]	72.6	225, 354, 377, 526, 611, 872, 1029, 1036, 1119, 1467, 2102, 3130, 3236, 3366
TS(2/5)[c]	72.6	188, 335, 401, 519, 589, 857, 1032, 1125, 1151, 1483, 1996, 3127, 3240, 3359
TS(3/5)[c]	72.6	340, 364, 549, 633, 649, 803, 1041, 1073, 1112, 1464, 2136, 3121, 3226, 3391

[a]See Scheme 1.
[b]Relative energies calculated with respect to allene cation with zero-point energy correction.
[c]**TS(1/5)**, **TS(2/5)**, and **TS(3/5)** represent the transition state for H dissociation from **1**, **2**, and **3** to produce **5**. The vibrational frequencies for these three TS were determined by elongating a C–H bond of allene cation, vinylmethylene cation, and propyne cation to 2 Å

Results and discussion

Structures and energetics

The PES for the isomerisation and fragmentation of allene cation ($H_2C=C=CH_2^+$) has been studied previously by Mebel and Bandrauk using the CCSD(T) calculations [9]. In the present work, the energetics of allene cation PES are calculated at the B3LYP/6-31 + G(d,p) level of theory and summarised in Figure 1. As shown in the previous study by Mebel and Bandrauk, there are four stable $C_3H_4^+$ structures: allene cation (1), vinylmethylene cation (2), propyne cation (3), and cyclopropene cation (4). The most stable $C_3H_4^+$ structure is allene cation (1) with a calculated dihedral angle of 49.6 degrees between the two CH_2 planes. A 1,2 hydrogen migration in allene cation leads to the formation of vinylmethylene cation (2), which is 25.5 kcal/mol higher than allene cation. The transition state for 1,2 hydrogen migration has a planar geometry and is 31.3 kcal/mol above allene cation. Vinylmethylene cation can undergo cyclisation with a very small energy barrier of 2.2 kcal/mol to form cyclopropene cation (4, which is 24.1 kcal/mol higher than allene cation) or return to allene cation with a small barrier of 5.8 kcal/mol. The 1,3 migration of hydrogen in allene cation has an energy barrier of 40.6 kcal/mol for the formation of propyne cation (3), which is 16 kcal/mol higher than the allene cation. The transition state for 1,3 hydrogen migration has a nonplanar geometry where the hydrogen moving above the middle carbon is perpendicular to the $H_2C=C=CH^+$ plane. Propyne cation can also be converted to cyclopropene cation, but this step

has a high energy barrier of 58.9 kcal/mol. In addition to isomerisation, there are three dissociation channels: loss of hydrogen to form H_2CCCH^+ (5, 72.6 kcal/mol higher than 1), loss of hydrogen from cyclopropene cation to form c-$C_3H_3^+$ (6, 23.6 kcal/mol higher than 4), and loss of H_2 from propyne cation to produce $HCCCH^+$ (7, 52.7 kcal/mol higher than 3). The relative energies of isomers and transition states calculated using B3LYP/6-31 + G(d,p) are 3–7 kcal/mol higher than the CCSD(T) calculations of Mebel and Bandrauk, but this is acceptable for the ab initio MD simulations in this study.

Dynamics

To simulate the isomerisation and fragmentation of allene cation by intense 7 μm laser pulses, the ab initio MD trajectories were calculated on the ground state surface using the B3LYP/6-31 + G(d,p) level of theory and were initiated from the optimised geometry of allene cation. When the laser field interacts with the molecule, considerable amounts of energy can be deposited in the vibrational modes. To explore the interaction of the laser with the molecule, simulations were carried out with various laser polarisations, field strengths, and pulse durations. For each set of laser pulses, 50 trajectories were initially calculated for 500 fs, and additional 150 trajectories were calculated if the first 50 trajectories exhibited chemical events during the 500 fs simulation time. The distributions and average amounts of energy gained from laser pulses with different parameters are presented in Figure 2 and Table 2. Figure 2 shows that
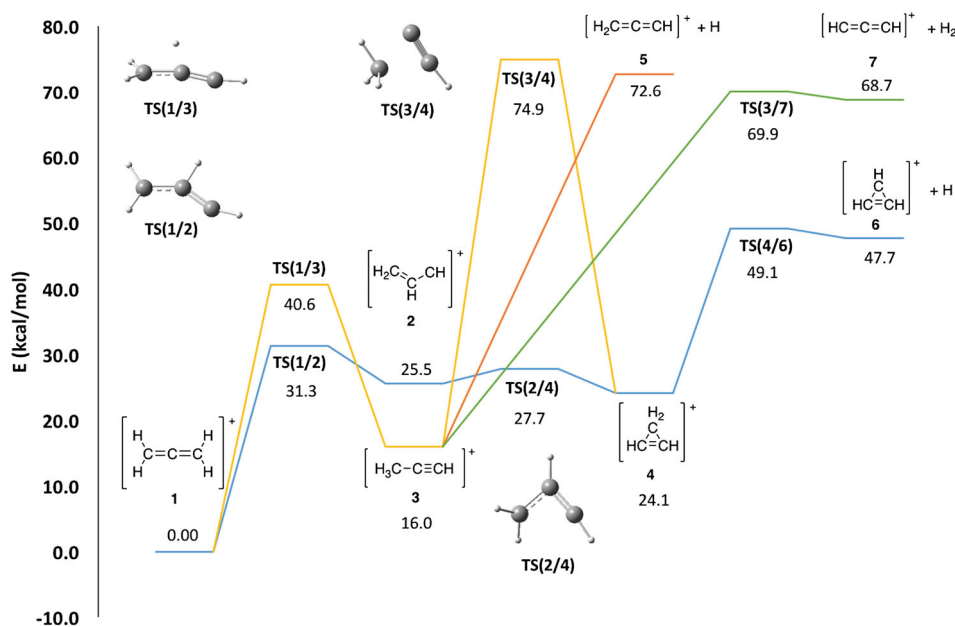

Figure 1. The PES of allene cation calculated at the B3LYP/6-31 + G(d,p) level of theory. The relative energies with respect to allene cation are calculated with zero-point energy correction.
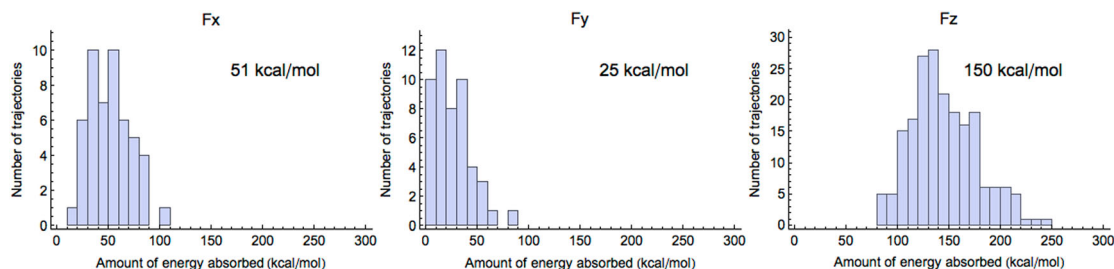
Figure 2. Histograms of the distribution of energy absorbed by allene cation for different polarisations of laser field: (a) Fx, (b) Fy, and (c) Fz. The definition of Fx, Fy, and Fz are shown in Figure 3.

Table 2. Number of trajectories of isomers and fragments obtained with BOMD using 7 μm laser pulses with a maximum field strength of 0.07 au.

Structure[a]	3-cycle[d] 85 kcal/mol[e] No.	5-cycle[d] 125 kcal/mol[e] No.	10-cycle[d] 150 kcal/mol[e] No.
1[b]	106 (51)	113 (19)	94 (15)
2	14	22	29
3	0	11	8
4	10	12	11
5[c]	11 (6)	7 (11)	19 (5)
6	2	2	14
7	0	2	3
Total	200	199	198

[a]See Scheme 1.
[b]The values represent number of trajectories of allene cation with rearranged hydrogens or carbons at 500 fs, and the values in parenthesis represent the number of unreactive trajectories throughout 500 fs simulation time.
[c]The values represent number of trajectories of $H_2CCCH^+ + H$ produced after isomerisation, and the values in parenthesis represent the number of trajectories undergoing direct H dissociation from allene cation before isomerisation.
[d]Pulse length.
[e]Energy gained from the laser pulse.

the allene cation with the laser polarisation aligned with the $C=C=C$ axis gained the most energy (150 kcal/mol) compared to the other two polarisations perpendicular to the $C=C=C$ axis (25 kcal/mol and 51 kcal/mol) with the same maximum field strength of 0.07 au. This can be

understood in terms of the IR spectrum of allene cation. Figure 3 shows that the frequency distribution for a 10 cycle 7 μm laser pulse is centred around 1430 cm^{-1} with a full width at half maximum (FWHM) of $\sim 200\ cm^{-1}$. This overlaps primarily with the vibrational modes in the region of 1300–1600 cm^{-1} which are linearly polarised along the $C=C=C$ axis of allene cation. The frequency at 1359 cm^{-1} corresponds to the bending motion of CH_2 groups in allene cation, and this vibration can facilitate the hydrogen migration within allene cation.

The results of trajectory calculations with 7 μm laser pulses are summarised in Table 2. The fraction of reactive trajectories depends on the amount of energy deposited in the molecule. Alignment of the laser field with the $C=C=C$ axis results in a higher percentage of trajectories undergoing isomerisation and fragmentation reactions because of the large amount of energy absorbed from the laser pulse. Most of the isomerisation and fragmentation occurs after the laser pulse. On the other hand, no isomerisation or bond dissociation was seen when the laser polarisation is perpendicular to the $C=C=C$ axis of allene cation because of the smaller amount of energy gained from the pulse. Therefore, the present study focusses on ab initio classical trajectories
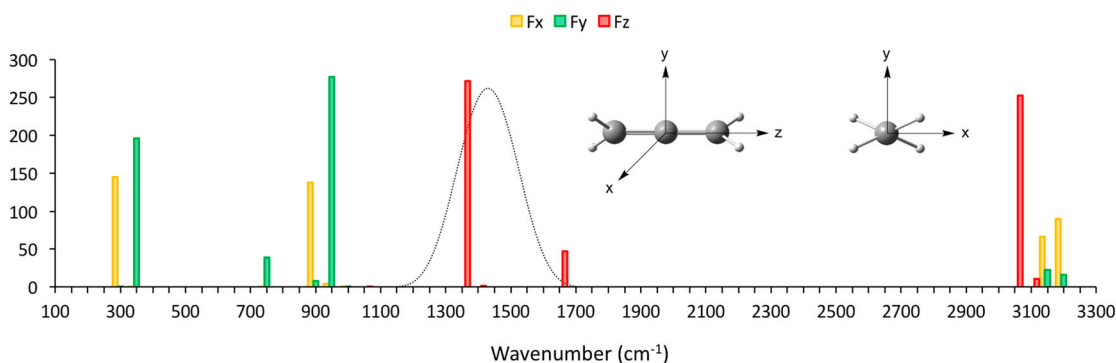

Figure 3. IR spectrum of allene cation when the light is linearly polarized along different molecular axes (Fx, Fy, Fz), and the frequency distribution for a 10-cycle 7 micron laser pulse (dotted line).

calculated with the laser field aligned with the C=C=C axis.

The branching ratio of all isomers and fragmentation products for a simulation time of 500 fs are listed in Table 2. As expected from the PES of allene cation, allene cation has the highest abundance (55%) because allene cation is the most stable $C_3H_4^+$ structure. The distribution of allene cation (55%) includes 8% of unreactive trajectories and 47% of reactive trajectories involving one or multiple steps of isomerisations. For these reactive trajectories of allene cation, approximate 18% show rearrangement of the C=C=C skeleton resulting from the formation of cyclopropene cation (**4**) and subsequent ring-opening, while the remaining 29% show only hydrogen migration. For isomerisation pathways, the percentages of vinylmethylene cation (**2**), propyne cation (**3**), and cyclopropene cation (**4**) are 15%, 4%, and 6%, respectively. Vinylmethylene cation (**2**) has higher branching ratio than propyne cation (**3**) and cyclopropene cation (**4**) because isomerisation to **2** involves a lower barrier for isomerisation and fewer intermediate steps. In addition, considerable rearrangement of the CCC skeleton is observed in vinylmethylene cation (**2**) and propyne cation (**3**) because of the formation of cyclopropene cation (**4**) as an intermediate. For formation of cyclopropene cation (**4**), trajectories show that all cyclopropene cation are converted from vinylmethylene cation (**2**) rather than propyne cation (**3**) because of the lower barrier for conversion from vinylmethylene cation to cyclopropene cation.

There are three dissociation channels to produce **5**, **6**, and **7**. Dissociation to $H_2CCCH^+ + H$ (**5**) is the dominant pathway (12%) in all dissociation reactions with a 10-cycle 7 μm laser pulse with the field strength of 0.07 au. For this type of dissociation, hydrogen can dissociate directly from allene cation without undergoing isomerisation (2%), or dissociate after isomerisation (10%) to vinylmethylene cation (**2**) or propyne cation (**3**). Hydrogen dissociation can also occur after formation of cyclopropene cation (**4**) to produce $c\text{-}C_3H_3^+ + H$ (**6**), which is the second most abundant dissociation channel (7%). Finally, propyne cation can eliminate H_2 to produce $HCCCH^+ + H_2$, but the fraction of this fragmentation reaction is relatively small (2%) compared to $H_2CCCH^+ + H$ (**5**, 12%) and $c\text{-}C_3H_3^+ + H$ (**6**, 7%).

The distribution of isomers and dissociation products is related to the amount of energy deposited in the molecules. The amount of energy deposited can be controlled by the pulse intensity and duration. The effect of pulse duration on the distribution of energy gained by the molecules is graphically presented in Figure 4, and the branching ratios for isomerisation and fragmentation are summarised in Table 2. Figure 4 and Table 2 show that the longer pulse can deposit more energy in the molecules, leading to more isomerisation and fragmentation. A 3-cycle 7 μm laser pulse deposits 85 kcal/mol, which is much less than the energy gained from a 5-cycle (125 kcal/mol) and a 10-cycle 7 μm laser pulse (150 kcal/mol) with the same field strength of 0.07 au. Therefore, the percentage of the reactive trajectories is less for a 3-cycle laser pulse compared to the 5-cycle and 10-cycle pulses. In addition, isomerisation to propyne cation (**3**) was observed for the 5-cycle and 10-cycle pulses but not for a 3-cycle 7 μm laser pulse

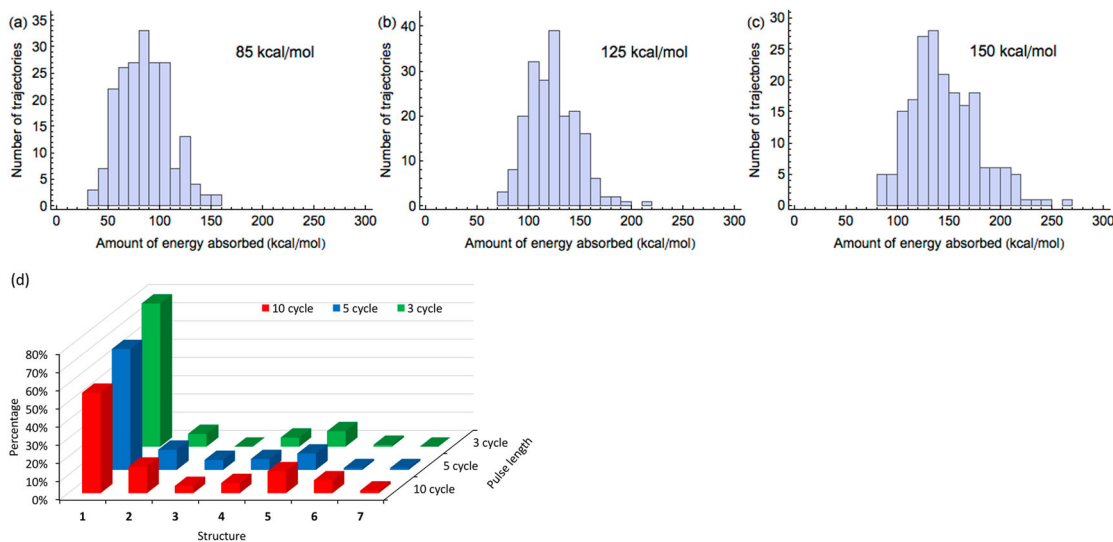**Figure 4.** Histograms of the distribution of energy absorbed by allene cation from (a) 3-cycle, (b) 5-cycle, and (c) 10-cycle 7 μm laser pulses. (d) The distribution of all isomers and fragments at the simulation time of 500 fs.

because 1,3 hydrogen migration has a higher energy barrier (40.6 kcal/mol) compared to 1,2 hydrogen migration (31.3 kcal/mol). Likewise, no H_2 elimination was found for a 3-cycle 7 μm laser pulse because insufficient energy was deposited in the molecule.

To compare with the branching ratio obtained with intense 7 μm laser pulses, field-free BOMD trajectories of allene cation were simulated with the same amount of energy as that absorbed from the laser, and the branching ratios are listed in Table 3. As expected, more energy deposited in the molecule results in more reactive trajectories for isomerisation and fragmentation. We found that with 150 kcal/mol energy, all trajectories undergo isomerisation or fragmentation during simulation. Allene cation has the highest population (34%)

Table 3. Number of trajectories of isomers and fragments with field-free BOMD using thermal energy equivalent to that gained from the 7 μm laser pulses.

Structure[a]	85 kcal[b] No.	125 kcal[c] No.	150 kcal[d] No.
1	157	115	68
2	24	19	29
3	7	9	10
4	10	13	19
5	1	35	46
6	1	6	14
7	0	0	13
Total	200	197	199

[a]See Scheme 1.
[b]The average amount of energy gained from a 3-cycle 7 μm pulse.
[c]The average amount of energy gained from a 5-cycle 7 μm pulse.
[d]The average amount of energy gained from a 10-cycle 7 μm pulse.

at 500 fs. For the other three isomers, the population of vinylmethylene cation, (**2**, 15%) is higher than propyne cation (**3**, 5%) and cyclopropene cation (**4**, 10%). For the three dissociation channels, the percentages of $H_2CCCH^+ + H$ (**5**), $c-C_3H_3 + H$ (**6**), and $HCCCH^+ + H_2$ (**7**) are 23%, 7%, and 6.5%, respectively. The branching ratio for **5** is dominant, consistent with the BOMD result for a 10-cycle 7 μm laser pulse. However, the percentages of **5** and **7** for field-free BOMD are higher compared to those for a 10-cycle 7 μm laser pulse (12% for **5** and 1.5% for **7**). In general, the branching ratios for field free BOMD are in good agreement with those induced by the laser pulses, which favours 1,2 hydrogen migration followed by H dissociation (**5** and **6**) over 1,3 hydrogen migration followed by H_2 elimination (**7**). For field-free BOMD, isomerisation starts from ∼20 fs. For BOMD in the presence of a 10-cycle 7 μm pulse, isomerisation does not starts until the second half of the pulse (160–200 ps) when enough energy has been deposited (an average of 115 kcal/mol by 160 fs and 139 kcal/mol by 200 fs). This suggests that the laser field needs to reach its maximum in order to drive the molecular vibrations and to deposit energy in the molecule so that isomerisation can occur.

RRKM calculation

For comparison with the BOMD results, the branching ratio for all isomers and dissociation products were also estimated by the RRKM calculations. The vibrational data and relative energies of all intermediates and
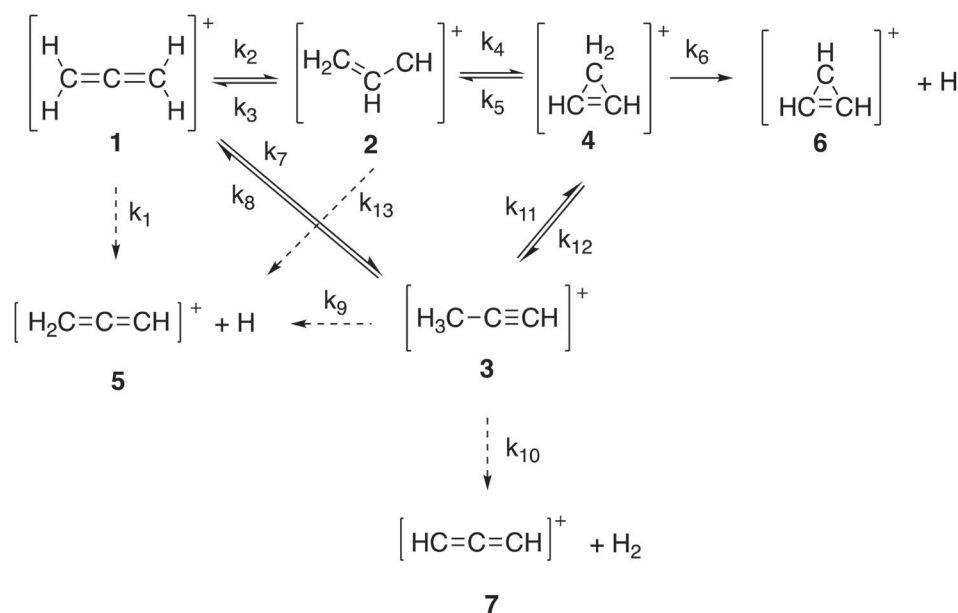
Scheme 1. Possible reaction pathways used in the RRKM calculation.

transition states in Figure 1 were used to calculate the rate constants for individual steps in isomerisation and dissociation reactions shown in Scheme 1. For isomerisation reactions, the forward and backward reactions are considered. For dissociation pathways, only the forward rate constant is taken into account for the RRKM calculations. For loss of hydrogen from **1**, **2**, and **3**, the vibrational frequencies of the transition states for these reaction channels were estimated by elongating the C–H bond distance of the optimised **1**, **2**, and **3** structures to 2 Å (similar to the distance in **TS(4/6)** in Figure 1) and calculating the frequencies with B3LYP/6-31 + G(d,p). The RRKM rate constants were calculated with the internal energy of allene cation corresponding to each set of laser condition using the averaged energy gained by the molecule (RRKM1) or weighted by the distribution of energy absorbed by the molecule shown in Figure 4(b–d) (RRKM2). The rate expressions are then integrated using the RRKM1 and RRKM2 rate constants to obtain the relative abundance of the isomers and dissociation products after 500 fs. The branching ratios calculated with the RRKM1 and RRKM2 rate constants are shown in Figure 5.

Figure 5 and Tables 4–6 show the RRKM branching ratios at 500 fs with three different internal energies: 85, 125, and 150 kcal/mol, which correspond to the averaged energy absorbed from 3-, 5-, and 10-cycle 7 μm laser pulses, respectively. At a lower internal energy of 85 kcal/mol (i.e. the energy distribution for a 3-cycle 7 μm laser pulse), the dominant species is propyne cation (**3**) with a percentage of 23.7% for RRKM1 and 21.1% for RRKM2. When the internal energy is increased to 150 kcal/mol (i.e. the energy distribution for a 10-cycle 7 μm laser pulse), the percentage of propyne cation (**3**) decreases to 7.4% for RRKM1 and 18.5% for RRKM2, and the branching ratio for H_2 elimination (**7**) increases to 57.9% for RRKM1 and 39.6% for RRKM2.

Tables 4–6 also summarise the comparison of RRKM results with BOMD in a laser field and field-free BOMD. For range of internal energies considered, the RRKM calculations favour the isomerisation to H_3CCCH^+ (**3**) and the dissociation to $HCCCH^+ + H_2$ (**7**), whereas for the BOMD calculations in the laser field and field-free, the dominant channels are 1,2 hydrogen migration to form $H_2C=CH–CH^+$ (**2**) and the dissociation to $H_2CCCH^+ + H$ (**5**) and c-$C_3H_3^+ + H$ (**6**). The RRKM calculations assume that the vibrational energy is redistributed statistically at every step in the reaction mechanism, whereas the BOMD calculations do not make this assumption, and the non-statistical energy distribution is a result of the classical trajectory calculations. Thus, the differences between the RRKM and BOMD branching ratios indicates that the intramolecular vibrational
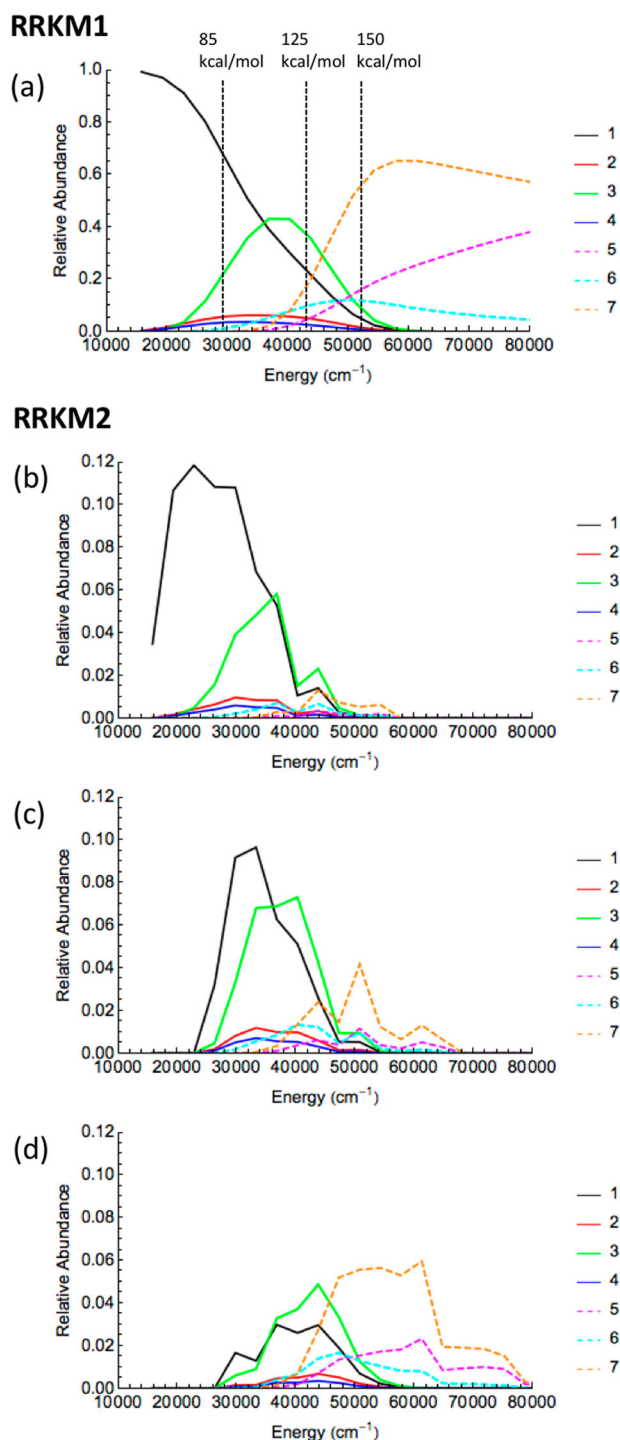

Figure 5. (a) Branching ratios as a function of energy using rate constants calculated by the RRKM, indicating the average energy deposited by 3-, 5- and 10-cycle 7 μm laser pulses (RRKM1). (b), (c) and (d) show the branching ratios as a function of energy weighted the energy distributions in Figure 4 for 3-, 5-, and 10-cycle laser pulses; the integral under each curve gives the total branching ratios listed under RRKM2 in Tables 4–6, respectively. All branching ratios are calculated at a simulation time of 500 fs.

redistribution in the intermediate isomers is not complete for the rapid isomerisation and fragmentation of allene cation in an intense laser field.

Table 4. The RRKM branching ratios (%) for isomers and fragments (**1–7**) with the internal energy of 85 kcal/mol, in comparison with BOMD in the present of a 3-cycle 7 μm laser pulse as well as field-free BOMD.

Structure[a]	BOMD with field (%)	Field-free BOMD (%)	RRKM1[b] (%)	RRKM2[c] (%)
1	78.5	78.5	65.6	62.7
2	7.0	12.0	5.8	4.5
3	0.0	3.5	23.7	21.1
4	5.0	5.0	3.6	2.7
5	8.5	0.5	0	1.0
6	1.0	0.5	1.3	2.8
7	0.0	0.0	0	3.8

[a] See Scheme 1.
[b] The branching ratios are obtained using the averaged amount of energy gained from a 3-cycle 7 μm laser pulse as the internal energy.
[c] The branching ratios are weighted by the distribution of energy absorbed from a 3-cycle 7 μm laser pulse.

Table 5. The RRKM branching ratios (%) for isomers and fragments (**1–7**) with the internal energy of 125 kcal/mol, in comparison with BOMD in the present of a 5-cycle 7 μm laser pulse as well as field-free BOMD.

Structure[a]	BOMD with field (%)	Field-free BOMD (%)	RRKM1[b] (%)	RRKM2[c] (%)
1	66.3	58.4	21.7	37.2
2	11.1	9.6	5.0	5.1
3	5.5	4.6	35.6	31.1
4	6.0	6.6	2.5	2.9
5	9.0	17.8	5.1	4.0
6	1.0	3.0	10.2	6.2
7	1.0	0.0	20.0	13.6

[a] See Scheme 1.
[b] The branching ratios are obtained using the averaged amount of energy gained from a 5-cycle 7 μm laser pulse as the internal energy.
[c] The branching ratios are weighted by the distribution of energy absorbed from a 5-cycle 7 μm laser pulse.

Table 6. The RRKM branching ratios (%) for isomers and fragments (**1–7**) with the internal energy of 150 kcal/mol, in comparison with BOMD in the present of a 10-cycle 7 μm laser pulse as well as field-free BOMD.

Structure[a]	BOMD with field (%)	Field-free BOMD (%)	RRKM1[b] (%)	RRKM2[c] (%)
1	55.1	34.2	4.1	14.4
2	14.6	14.6	1.4	2.8
3	4.0	5.0	7.4	18.5
4	5.6	9.5	0.7	1.5
5	12.1	23.1	16.7	14.2
6	7.1	7.0	11.8	9.1
7	1.5	6.5	57.9	39.6

[a] See Scheme 1.
[b] The branching ratios are obtained using the averaged amount of energy gained from a 10-cycle 7 μm laser pulse as the internal energy.
[c] The branching ratios are weighted by the distribution of energy absorbed from a 10-cycle 7 μm laser pulse.

Conclusions

The PES of allene cation has been studied at the B3LYP/6-31 + G(d,p) level of theory. The energetics show that allene cation can isomerise to $H_2C=CH–CH^+$, H_3CCCH^+, and cyclopropene cation, and these intermediate isomers can dissociate to $H_2CCCH^+ + H$, c-$C_3H_3^+ + H$, and $HCCCH^+ + H_2$. To simulate the branching ratios for isomerisation and fragmentation reactions of allene cation in a laser field, the trajectories were calculated on the ground state Born-Oppenheimer surface in the presence of a 10-cycle 7 μm laser pulse with maximum field strength of 0.07 au. No isomerisation and fragmentation occurred when the field was perpendicular to the $C=C=C$ bond of allene cation because too little energy was deposited (25 kcal/mol and 51 kcal/mol). Compared to perpendicular orientations, allene cation absorbed considerable amount of energy when the field is aligned with the $C=C=C$ axis (ca. 150 kcal/mol). Approximately 90% of the trajectories for aligned allene cation underwent one or more structural rearrangement steps to form various isomers such as $H_2C=CH–CH^+$ (15%), H_3CCCH^+ (4%), cyclopropene cation (6%), and allene cation (47%) with rearranged hydrogens and carbons. In addition, a variety of fragments including $H_2CCCH^+ + H$ (10%), c-$C_3H_3^+ + H$ (7%), and $HCCCH^+ + H_2$ (2%) were produced from various isomers. The BOMD results favour the isomerisation to $H_2C=CH–CH^+$ and the dissociation to $H_2CCCH^+ + H$ and c-$C_3H_3^+ + H$. However, RRKM calculations favour the isomerisation to propyne cation and the dissociation to $HCCCH^+ + H_2$. This is because the intramolecular vibrational redistribution in the intermediate isomers is not complete before the next isomerisation or fragmentation reactions occur. This suggests that non-statistic dynamics is important for the studies of isomerisation and fragmentation of molecules in intense laser fields.

References

[1] K. Hoshina, Y. Furukawa, T. Okino and K. Yamanouchi, J. Chem. Phys. **129**, 104302 (2008).
[2] T. Okino, A. Watanabe, H.L. Xu and K. Yamanouchi, Phys. Chem. Chem. Phys. **14**, 10640 (2012).
[3] T. Okino, A. Watanabe, H.L. Xu and K. Yamanouchi, Phys. Chem. Chem. Phys. **14**, 4230 (2012).
[4] T. Okino and K. Yamanouchi, Springer Ser. Chem. Ph. **107**, 49 (2014).

[5] H. Xu, T. Okino and K. Yamanouchi, Chem. Phys. Lett. **469**, 255 (2009).

[6] H.L. Xu, T. Okino, K. Nakai and K. Yamanouchi, *Prog. Ultrafast Intense Laser Sci.* **100**, 35 (2011).

[7] H.L. Xu, T. Okino and K. Yamanouchi, J. Chem. Phys. **131**, 151102 (2009).

[8] H.L. Xu, T. Okino and K. Yamanouchi, Appl. Phys. A **104**, 941 (2011).

[9] A.M. Mebel and A.D. Bandrauk, J. Chem. Phys. **129**, 224311 (2008).

[10] S.K. Lee, H.B. Schlegel and W. Li, J. Phys. Chem. A **117**, 11202 (2013).

[11] S.K. Lee, A.G. Suits, H.B. Schlegel and W. Li, J. Phys. Chem. Lett. **3**, 2541 (2012).

[12] X.T. Shi, B. Thapa, W. Li and H.B. Schlegel, J. Phys. Chem. A **120**, 1120 (2016).

[13] B. Thapa and H.B. Schlegel, J. Phys. Chem. A **118**, 10067 (2014).

[14] B. Thapa and H.B. Schlegel, Chem. Phys. Lett. **610**, 219 (2014).

[15] B.T. Psciuk, P. Tao and H.B. Schlegel, J. Phys. Chem. A **114**, 7653 (2010).

[16] M.J. Frisch, G.W. Trucks, H.B. Schlegel, G.E. Scuseria, M.A. Robb, J.R. Cheeseman, G.B.V. Scalmani, B. Mennucci, G.A. Petersson, H. Nakatsuji, et al., *Gaussian Development Version, Revision I.06* (Gaussian, Inc., Wallingford, CT, 2016).

[17] H.B. Schlegel, J. Chem. Theory Comput. 9, 3293 (2013).

[18] V. Bakken, J.M. Millam and H.B. Schlegel, J. Chem. Phys. **111**, 8773 (1999).

[19] H. Wu, M. Rahman, J. Wang, U. Louderaj, W.L. Hase and Y. Zhuang, J. Chem. Phys. **133**, 074101 (2010).

[20] D.L. Bunker and W.L. Hase, J. Chem. Phys. **59**, 4621 (1973).

[21] T. Beyer and D.F. Swinehart, Commun. ACM **16**, 379 (1973).